RAD Conference Proceedings, vol. 9, pp. 47-53, 2025
ISSN 2466-4626 (online) | DOI: 10.21175/RadProc.2025.09
www.rad-proceedings.org

OPTICAL AND MORPHOLOGICAL ANALYSIS OF GOLD NANOPARTICLES EXPOSED TO IONIZING RADIATION

Philip Marinov*[1,2], Ivo Petrov[2], Tsvetoslav Lazhovski[2], Krum Stoilov[2], Peter Temnishki[1], Silviya Simeonova[3], Peter Georgiev[3], Lyuben Mihaylov[3], Evelina Vassileva[3], Konstantin Balashev[3]

[1]Medical University- Pleven, Pleven, Bulgaria
[2]Heart and Brain Center of Excellence, Pleven, Bulgaria
[3]Sofia University, Sofia, Bulgaria

Abstract. *Gold nanoparticles (AuNPs) exhibit size-dependent optical properties governed by localized surface plasmon resonance (LSPR) and strong X-ray absorption, making them attractive for biomedical imaging and radiosensitization. Understanding their response to ionizing radiation is therefore essential. Here, citrate-stabilized AuNPs synthesized by the Turkevich method were exposed to LINAC photon irradiation at doses from 0.1 to 100 Gy and characterized by UV–Vis spectroscopy, AFM, and TEM. UV–Vis measurements showed a non-monotonic dose dependence of LSPR intensity with a maximum at 1 Gy, while no significant peak position shift was observed. AFM and TEM analyses revealed dose-dependent changes in nanoparticle size distribution and morphology. Quantitative statistical evaluation indicated particle growth at intermediate doses followed by redistribution toward smaller characteristic sizes at higher doses. These findings demonstrate that clinically relevant irradiation induces measurable but moderate modifications in AuNP optical and structural properties without pronounced aggregation, contributing to the understanding of radiation–nanoparticle interactions.*
Keywords: *Gold nanoparticles, ionizing radiation, UV–Vis spectroscopy, Atomic Force Microscopy (AFM), Transmission Electron Microscopy (TEM), surface plasmon resonance, morphology.*

1. INTRODUCTION

Gold nanoparticles (AuNPs) have attracted considerable attention in biomedicine due to their exceptional biocompatibility, chemical stability, and size-dependent optical properties arising from localized surface plasmon resonance (LSPR). This phenomenon enables strong light absorption and scattering, rendering AuNPs highly valuable in applications including bioimaging, photothermal therapy, and radiation enhancement strategies in oncology [1].

In radiotherapeutic contexts, AuNPs function as effective radiosensitizers primarily because of their high atomic number (Z = 79), which enhances local energy deposition via photoelectric absorption and Compton scattering processes [2]. These interactions result in the emission of secondary electrons, including Auger and photoelectrons, capable of amplifying nanoscale radiation damage. Furthermore, AuNPs may facilitate increased reactive oxygen species (ROS) generation, thereby contributing to enhanced cellular radiosensitivity. Their tunable size, adaptable surface chemistry, and favorable biological compatibility enable selective tumor targeting, supporting their role as multifunctional platforms for combined diagnostic and therapeutic applications [3,4].

Despite these advantages, exposure to ionizing radiation may induce structural, morphological, and electronic modifications in nanoparticles, potentially altering their physicochemical behavior, colloidal stability, and biological interactions [5,6]. Such radiation-induced effects are particularly relevant in clinical environments, where nanoparticles may be subjected to therapeutic radiation fields. Therefore, understanding dose-dependent nanoparticle transformations is essential for predicting nanoparticle performance, ensuring safety, and optimizing therapeutic efficacy.

The present study extends our previous work [7], by systematically investigating radiation-induced optical and morphological alterations of citrate-stabilized AuNPs exposed to clinically relevant LINAC irradiation doses. In contrast to earlier investigations primarily focused on qualitative observations, this work integrates quantitative UV–Vis spectroscopy with statistically robust Atomic Force Microscopy (AFM) and Transmission Electron Microscopy (TEM) analyses. Particular emphasis is placed on correlating LSPR behavior with nanoparticle size distribution and morphological evolution as a function of radiation dose. This comprehensive multimodal characterization provides deeper insight into the mechanisms governing radiation–nanoparticle interactions and contributes to a more reliable assessment of

* E-mail of the corresponding author– filip.marinov@mu-pleven.bg

nanoparticle stability under therapeutic irradiation conditions. Such understanding is critical for minimizing potential risks, including unintended aggregation, altered biodistribution, and long-term toxicity, while enabling the rational design of nanoparticle-based radiosensitization strategies.

The aim of this work is to quantitatively evaluate the effects of ionizing radiation on the optical response, morphology, and size distribution of citrate-stabilized gold nanoparticles (AuNPs) exposed to clinically relevant LINAC irradiation doses. Specifically, we investigate dose-dependent modifications of the localized surface plasmon resonance (LSPR) using UV–Vis spectroscopy and correlate these changes with nanoparticle geometrical parameters obtained from AFM and TEM analyses. Through statistically evaluation of nanoparticle dimensions and distributions, this study seeks to elucidate the mechanisms governing radiation-induced nanoparticle transformations and assess their implications for nanoparticle stability and radiosensitization performance.

We hypothesize that exposure of citrate-stabilized AuNPs to ionizing radiation induces dose-dependent modifications in their LSPR behavior arising from radiation-driven alterations in nanoparticle morphology, size distribution, and surface characteristics. These structural changes are expected to influence the nanoparticle optical response without necessarily causing significant aggregation or loss of colloidal stability at clinically relevant doses.

MATERIALS AND METHODS

Chemicals and Reagents. Gold(III) chloride hydrate ($HAuCl_4 \cdot xH_2O$) and trisodium citrate dihydrate ($Na_3C_6H_5O_7 \cdot 2H_2O$), both of analytical grade, were obtained from Merck (Germany) and used without further purification. All aqueous solutions were prepared using deionized water (resistivity ≥ 18.2 MΩ·cm).

Synthesis procedure. Gold nanoparticles (AuNPs) were synthesized following the classical Turkevich method [8,9]. Briefly, 10 mL of a 2.5 mM $HAuCl_4$ solution (containing approximately 5 mg of Au) was diluted with 85 mL of deionized water. The solution was stirred at 350 rpm and heated to 90 °C. Subsequently, 5 mL of a 1% (w/v) trisodium citrate solution was rapidly added under continuous stirring. The reaction mixture was maintained at 90 °C for 30 minutes. Nanoparticle formation was confirmed by the characteristic color change from pale yellow/blue to ruby red, indicating the development of localized surface plasmon resonance (LSPR).

Irradiation Procedure. AuNP dispersions were transferred into sealed 1.5 mL polypropylene Eppendorf tubes and irradiated using a Versa HD medical linear accelerator (Elekta AB, Sweden). Irradiation was performed with 6 MV flattened photon beams operating in service mode. To ensure reproducible dose deposition and electronic equilibrium conditions, the sample tubes were positioned at a depth of 10 cm inside a BluePhantom2 water phantom (IBA Dosimetry, Germany). The setup was aligned at the LINAC isocenter with a source-to-surface distance (SSD) of 90 cm.

Figure 1. Linear accelerator (LINAC) setup used for irradiation of AuNP solutions. *Inset:* sample holder positioned within the water phantom during irradiation.

Treatment planning was conducted using the Monaco 5.51 planning system. Delivered doses were independently verified using an FC65-G Farmer ionization chamber coupled with a Dose1 electrometer (IBA Dosimetry, Germany).

UV–Visible Absorption Spectroscopy. UV–Visible absorption spectra were recorded using an Evolution 300 spectrophotometer (Thermo Scientific, USA) approximately one-hour post-irradiation. Measurements were performed using microvolume quartz cuvettes with a fixed optical path length. Samples were analyzed without dilution. Spectra were acquired over the wavelength range of 400–800 nm. Baseline correction was performed using deionized water as a reference.

AFM Sample Preparation and Imaging. For Atomic Force Microscopy (AFM) analysis, aliquots of AuNP dispersions were deposited onto freshly cleaved mica substrates. Following spin-coating, samples were dried under a gentle nitrogen stream. AFM imaging was conducted using a NanoScope V system (Bruker, USA) operating in tapping mode at room temperature.

Silicon cantilevers with aluminum reflex coatings (nominal tip radius < 10 nm; resonance frequency

~150 kHz) were employed. Images were acquired at 512 × 512 pixel resolution. Background flattening and leveling were performed using Gwyddion 2.70 software.

Nanoparticle dimensions were extracted via grain analysis. Particle height was defined as the maximum grain value, while lateral dimensions were evaluated using the equivalent disc radius. Tip-convolution effects were considered during diameter estimation.

TEM Sample Preparation and Imaging. For Transmission Electron Microscopy (TEM), AuNP dispersions were drop-cast onto carbon-coated copper grids and allowed to dry under ambient conditions. Imaging was performed using a JEM-2100 LaB_6 transmission electron microscope (JEOL, Japan). Nanoparticle size analysis was conducted using Fiji (ImageJ).

Equivalent circular diameters were calculated from segmented particle areas. Objects below 2 nm were excluded due to segmentation limitations at the noise/contrast threshold.

Statistical Analysis. Nanoparticle size distributions obtained from AFM and TEM measurements were analyzed using Microsoft Excel (Microsoft Corp., USA). Histograms were constructed using fixed bin widths selected according to the Freedman–Diaconis criterion where applicable.

Size distributions were evaluated assuming log-normal behavior. The reported statistical descriptors include mean diameter, median diameter, and standard deviation, together with log-normal fitting parameters (μ, σ).

AFM-based size analysis was performed on datasets containing approximately 250 to 450 nanoparticles per sample, depending on image quality and segmentation reliability. The largest dataset comprised 465 nanoparticles. TEM particle counts varied according to image resolution and thresholding constraints.

3. Results and Discussion

In contrast to previous reports describing negligible radiation-induced effects in ~20 nm Turkevich-synthesized AuNPs at doses near 2 Gy [5], the present study demonstrates measurable dose-dependent modifications in the optical response of citrate-stabilized AuNPs. These differences may partly arise from the slightly smaller nanoparticle diameter obtained in our synthesis (~16 nm, data not shown). The observed optical changes are supported by UV–Vis spectroscopy and further examined by AFM and TEM analyses.

The optical properties of the AuNP dispersions were evaluated using UV-Vis absorption spectroscopy following LINAC photon irradiation at doses ranging from 0.1 to 100 Gy (Figure 2A). All spectra display a well-defined localized surface plasmon resonance (LSPR) band centered near 520–525 nm, characteristic of predominantly spherical gold nanoparticles. Importantly, no significant shift in the LSPR peak position was detected across the investigated dose range.

After baseline correction using the absorbance at 780 nm as an estimate of the scattering/background contribution, the non-irradiated reference sample exhibited a very low long-wavelength tail ($A^*(650)/A^*(520) \approx 0.011$), consistent with a well-dispersed AuNP system. In contrast, all irradiated samples displayed increased tail ratios (approximately 0.09–0.10), indicating enhanced long-wavelength extinction attributable to increased scattering and/or weak interparticle plasmonic coupling. Notably, the tail ratios remained comparable across irradiation doses, suggesting the absence of pronounced dose-dependent aggregation effects within the irradiated series.

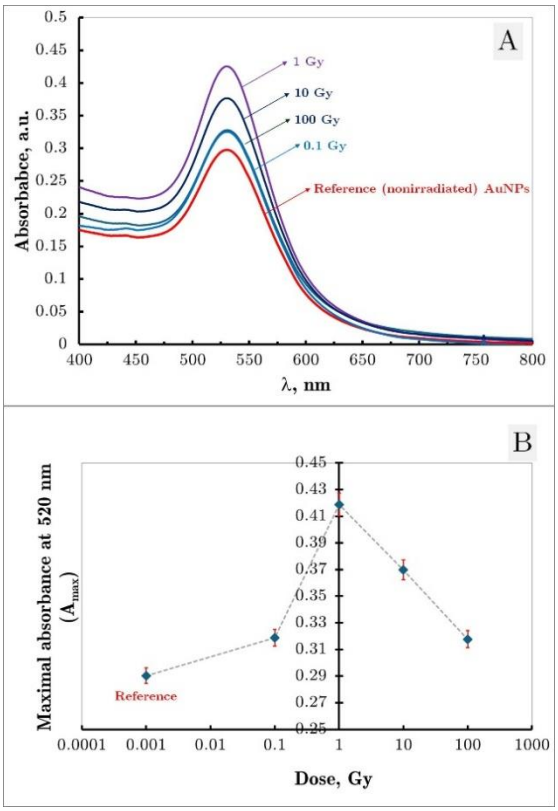

Figure 2. (A) UV–Vis absorption spectra of citrate-stabilized AuNP dispersions following LINAC photon irradiation at doses between 0.1 and 100 Gy. (B) Dose dependence of maximal absorbance at 520 nm (A_{max}), illustrating nonlinear optical response behavior.

The maximal absorbance at 520 nm (A_{max}) (Figure 2B) exhibited a nonlinear dose dependence, with a pronounced maximum at approximately 1 Gy. Even the lowest irradiation dose (0.1 Gy) produced a slight increase in absorbance relative to the reference sample. This enhancement became most prominent at 1 Gy, while higher doses (10–100 Gy) resulted in a gradual reduction in absorbance, although values remained above the control level. A similar non-monotonic trend was observed for the integrated spectral intensity (AUC).

The preservation of the LSPR peak position indicates that the fundamental plasmonic characteristics of the nanoparticles remain largely unchanged, implying the absence of extensive aggregation or drastic shape transformations. The observed variations in absorbance intensity and moderate peak broadening are consistent with subtle modifications in nanoparticle size distribution, surface structure, or local dielectric environment. Such effects may originate from radiation-induced alterations in surface chemistry or minor nanoparticle restructuring rather than large-scale particle coalescence.

Considering the well-established sensitivity of LSPR features to nanoparticle dimensions, morphology, and interparticle interactions [10], the detected spectral variations provide indirect evidence of radiation-driven nanoscale modifications. Although no significant shift in the LSPR peak position was observed, subtle changes in peak intensity and bandwidth may reflect radiation-induced alterations at the nanoparticle surface. Ionizing radiation is known to generate reactive species capable of modifying ligand structure, surface charge, and local electronic states. Consequently, minor changes in the oxidation state of surface atoms or in Au–ligand interactions cannot be excluded [11]. Such effects may influence the local dielectric environment and plasmon damping without requiring large-scale aggregation or pronounced morphological transformation. These considerations are important for evaluating the physicochemical stability of AuNPs under irradiation conditions relevant to biomedical applications. The proposed interpretations are further examined through direct morphological characterization using AFM and TEM.

To further investigate the radiation-induced modifications suggested by the UV-Vis analysis, AuNP dispersions were deposited onto freshly cleaved mica substrates and examined by Atomic Force Microscopy (AFM). Topographical measurements were acquired over representative 5 × 5 μm scan areas to assess nanoparticle morphology, spatial distribution, and size characteristics as a function of irradiation dose (Figure 3).

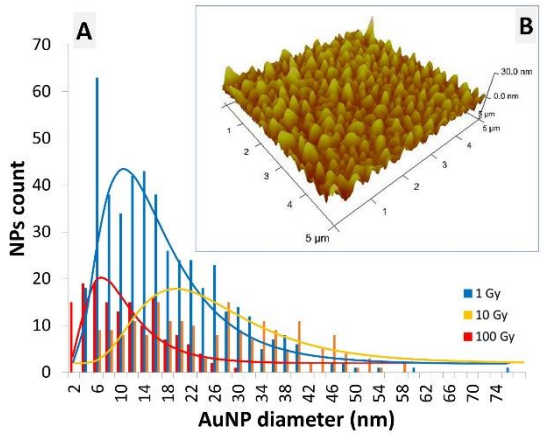

Figure 3. (A) Histograms showing nanoparticle size distributions derived from AFM grain analysis for AuNP samples irradiated with different LINAC photon doses (0.1, 1, and 100 Gy). Solid lines represent log-normal fits to the experimental distributions.
(B) Representative three-dimensional AFM topography image illustrating the surface morphology and spatial distribution of deposited AuNPs over a 5 × 5 μm scan area.

The non-irradiated reference sample (data not shown) exhibited well-dispersed, discrete nanoparticles with predominantly spherical morphology and minimal aggregation, confirming the high colloidal stability of the synthesized citrate-stabilized AuNPs. These observations are consistent with previous reports for Turkevich-derived nanoparticles [7,12] and provide a reliable baseline for evaluating radiation-induced structural alterations.

AFM analysis of irradiated samples revealed clear dose-dependent variations in nanoparticle topography and lateral dimensions. Representative three-dimensional AFM renderings are presented in Figure 3B. Although the overall nanoparticle morphology remained largely preserved, irradiation induced measurable modifications in particle size distribution and surface organization.

Quantitative grain analysis demonstrated that irradiation at lower doses (0.1–1 Gy) produced broader size distributions accompanied by the emergence of larger surface features. In contrast, samples exposed to higher doses (100 Gy) exhibited comparatively narrower distributions dominated by smaller particles. Statistical evaluation of equivalent nanoparticle diameters derived from AFM images (Figure 3A) confirms systematic differences between irradiation conditions.

Log-normal modeling of AFM-derived diameters revealed a non-monotonic dose dependence. Log-normal distribution parameters (μ, σ) were estimated by moment matching using the experimentally determined mean diameters and corresponding standard deviations. Between 0.1 Gy and 1 Gy, the median diameter increased from 14.48 to 25.15 nm (+73.7%), the mean from 18.53 to 31.65 nm (+70.8%), and the mode from 8.85 to 15.88 nm (+79.5%). In contrast, at 100 Gy the distribution shifted toward smaller characteristic sizes (median 10.03 nm; mean 14.61 nm; mode 4.73 nm), corresponding to reductions of 53.8–70.2% relative to the 1 Gy sample. Concurrently, the multiplicative dispersion increased substantially (σ: 0.678 → 0.867; GSD: 1.97 → 2.38).

Notably, AFM-derived height distributions did not indicate extensive particle coalescence or large-scale aggregation. Instead, the observed variations are consistent with subtle restructuring processes, potentially involving radiation-induced modifications of nanoparticle surface chemistry, ligand configuration, or local particle rearrangement on the substrate.

These AFM observations are in good agreement with the UV–Vis results, which revealed dose-dependent variations in LSPR intensity and bandwidth without significant peak position shifts. A

direct comparison with TEM analysis is presented in the following section.

To complement the AFM analysis and provide independent verification of nanoparticle size and morphology, Transmission Electron Microscopy (TEM) was performed on AuNP dispersions subjected to LINAC photon irradiation. Representative TEM micrographs are shown in Figure 4A, including magnified regions highlighting smaller nanoparticle populations.

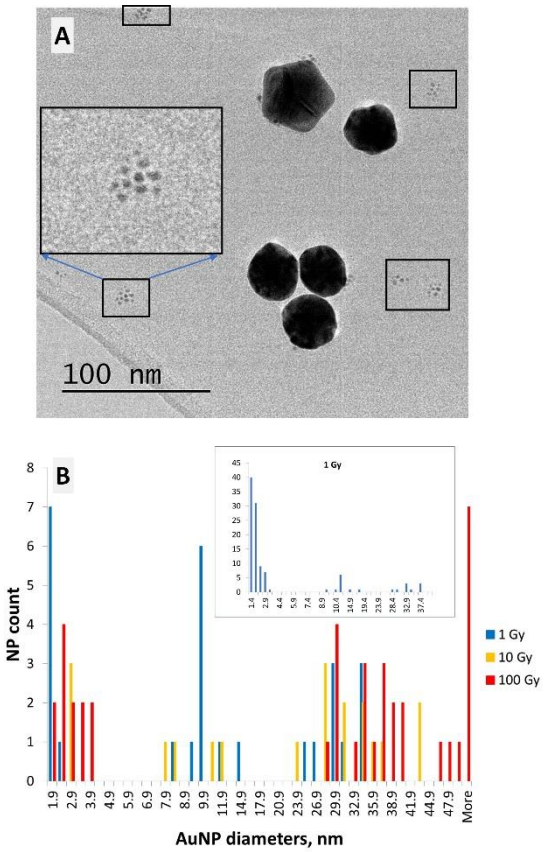

Figure 4. (A) Representative TEM micrograph of citrate-stabilized gold nanoparticles (AuNPs) following LINAC photon irradiation. Highlighted regions indicate areas selected for detailed size analysis, and the inset shows a magnified view of smaller nanoparticle clusters. Scale bar: 100 nm.
(B) Nanoparticle size distributions derived from TEM image analysis for selected irradiation doses. Particles smaller than 2 nm were excluded to minimize resolution-related uncertainties. The histograms illustrate the coexistence of multiple nanoparticle populations and dose-dependent variations in characteristic particle sizes.

The non-irradiated reference sample (data not shown) displayed predominantly spherical, well-separated nanoparticles with minimal aggregation, consistent with the expected morphology of citrate-stabilized Turkevich-synthesized AuNPs. These observations confirm that the initial colloidal system exhibited good structural integrity prior to irradiation.

TEM examination of irradiated samples revealed the coexistence of multiple nanoparticle populations. In addition to the dominant fraction of small nanoparticles, larger particles and irregularly shaped structures were occasionally observed. To ensure statistical reliability and minimize uncertainties associated with resolution limits and noise contributions, particles smaller than 2 nm were excluded from quantitative analysis.

Size distributions extracted from TEM images (Figure 4B) demonstrate dose-dependent variations consistent with the trends identified by AFM. Samples irradiated at lower doses exhibited broader distributions with an increased contribution of larger nanoparticles, whereas higher-dose samples showed distributions shifted toward smaller characteristic sizes. Although the distributions deviate from an ideal log-normal form due to the presence of multiple particle populations, systematic differences between irradiation conditions remain evident.

It is important to note that, unlike AFM specimens prepared immediately after irradiation, TEM samples were analyzed following a longer storage period necessitated by instrumental availability. Despite efforts to minimize environmental influences by storing samples at reduced temperature, this time lag may have contributed to partial restructuring, Ostwald ripening, or redistribution processes within the colloidal system. Such effects could enhance size polydispersity or modify relative population fractions.

Nevertheless, key morphological features remain consistent across TEM and AFM analyses. Both techniques indicate preservation of the predominant nanoparticle morphology, absence of extensive aggregation, and non-monotonic dose-dependent evolution of nanoparticle size characteristics. These observations align with the UV-Vis spectroscopy results, where variations in LSPR intensity and bandwidth were detected without significant peak position shifts.

Direct comparison of AFM and TEM analyses underscores the complementary nature of the two techniques. AFM measurements, performed on nanoparticles deposited on mica immediately after irradiation, provide three-dimensional topographical information, whereas TEM imaging yields high-resolution projections of dried nanoparticles on carbon-supported grids.

Despite inherent methodological differences, both techniques reveal consistent trends, including preservation of nanoparticle morphology, absence of extensive aggregation, and a non-monotonic dose dependence of size characteristics. Minor quantitative discrepancies between AFM- and TEM-derived diameters are attributed to differences in measurement principles, tip–sample convolution effects in AFM, and the time interval preceding TEM analysis. Overall, the agreement in qualitative features and dose-dependent tendencies strengthens the reliability of the observed radiation-induced nanoparticle modifications.

For improved visualization of the dose-dependent morphological evolution, Figure 5

summarizes the average equivalent diameters of the AuNPs derived from AFM grain analysis. The data reveal a clear non-monotonic dependence of nanoparticle size on irradiation dose.

Specifically, the mean equivalent diameter increases from the reference sample to 0.1 Gy and reaches a maximum near 1 Gy, followed by a gradual decrease at higher doses (10-100 Gy). This trend is consistent with the UV-Vis results, where maximal LSPR intensity was also observed at 1 Gy. The combined observations indicate that low-to-intermediate irradiation doses promote an apparent increase in nanoparticle dimensions, whereas higher doses favor redistribution toward smaller characteristic sizes.

Concurrently, qualitative inspection of AFM images shows a transition from predominantly spherical nanoparticles in the reference sample to more irregular and complex surface features at intermediate doses. At higher doses, nanoparticles exhibit a tendency toward more compact and near-spherical morphologies. This behavior suggests competing radiation-induced processes, potentially involving surface diffusion, ligand modification, and nanoparticle restructuring.

Despite the pronounced polydispersity observed at intermediate doses, the absence of significant height anomalies or large aggregates suggests that irradiation predominantly influences nanoparticle size distribution and morphology rather than inducing extensive aggregation. Consistently, the combined UV–Vis, AFM, and TEM analyses demonstrate that X-ray exposure leads to measurable modifications in the optical and structural characteristics of citrate-stabilized AuNPs. To further elucidate the mechanisms underlying these dose-dependent effects, future investigations employing complementary techniques—such as dynamic light scattering for hydrodynamic size assessment and high-resolution electron microscopy for detailed structural analysis—would be beneficial [10,13,14].

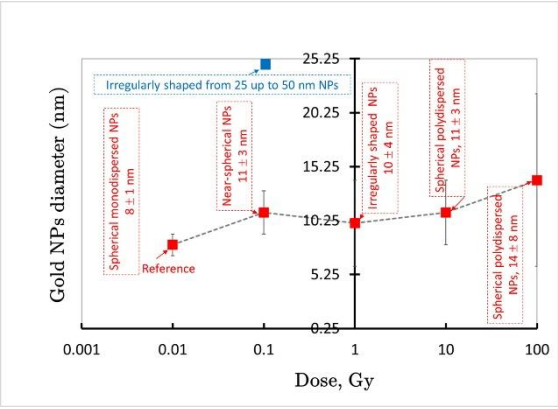

Figure 5. Dose-dependent variation of the average equivalent diameter of citrate-stabilized gold nanoparticles (AuNPs) obtained from AFM grain analysis. The dashed line serves as a guide to the eye. Representative nanoparticle morphologies characteristic of each irradiation dose are schematically indicated.

5. Conclusion

This study examined the effects of ionizing photon radiation delivered by a medical linear accelerator on citrate-stabilized gold nanoparticles synthesized via the classical Turkevich method. Radiation-induced modifications in nanoparticle optical response, morphology, and size distribution were quantitatively evaluated using UV-Vis spectroscopy, Atomic Force Microscopy (AFM), and Transmission Electron Microscopy (TEM).

UV-Vis analysis revealed a non-monotonic dose dependence of the localized surface plasmon resonance (LSPR) intensity, with maximal enhancement observed at 1 Gy relative to the non-irradiated reference. Importantly, no significant shift in the LSPR peak position was detected, indicating preservation of the fundamental plasmonic characteristics. Variations in spectral intensity and bandwidth suggest subtle radiation-induced changes in nanoparticle size distribution and local dielectric environment.

AFM and TEM measurements corroborated the spectroscopic findings, demonstrating dose-dependent alterations in nanoparticle dimensions and morphology. Quantitative log-normal analysis of AFM-derived diameters indicated particle growth at intermediate doses (0.1–1 Gy), followed by a redistribution toward smaller characteristic sizes and increased dispersion at higher doses (100 Gy). These observations suggest that irradiation influences nanoscale structural organization without inducing extensive aggregation.

Overall, the results confirm that clinically relevant photon irradiation can induce measurable modifications in AuNP optical and morphological properties. These findings are of particular relevance for biomedical applications involving nanoparticle exposure to therapeutic radiation fields. Future studies employing complementary techniques, such as dynamic light scattering, surface chemistry analysis, and in situ irradiation characterization, would be valuable for clarifying the mechanisms governing radiation–nanoparticle interactions and their implications for nanoparticle stability and performance.

***Acknowledgements*:** This study is financed by the European Union-NextGenerationEU, through the National Recovery and Resilience Plan of the Republic of Bulgaria, project № BG-RRP-2.004-0003.

References

1. M. Li, J. Wei, Y. Song, F. Chen, "Gold Nanocrystals: Optical Properties, Fine-Tuning of the Shape, and Biomedical Applications", *RSC Adv.*, vol. 12, pp. 23057–23073, 2022. https://doi.org/10.1039/D2RA04242H
2. A. Alhussan, E.P.D. Bozdoğan, D.B. Chithrani, "Combining Gold Nanoparticles with Other Radiosensitizing Agents for Unlocking the Full Potential of Cancer Radiotherapy", *Pharmaceutics,* vol. 13, no. 4, 442, 2021. https://doi.org/10.3390/pharmaceutics13040442

3. S. Her, D.A. Jaffray, C. Allen, "Gold Nanoparticles for Applications in Cancer Radiotherapy: Mechanisms and Recent Advancements", *Advanced Drug Delivery Reviews*, vol. 109, pp. 84–101, 2017. https://doi.org/10.1016/j.addr.2015.12.012
4. N.R.S. Sibuyi, K.L. Moabelo, A.O. Fadaka, S. Meyer, M.O. Onani, A.M. Madiehe, M. Meyer, "Multifunctional Gold Nanoparticles for Improved Diagnostic and Therapeutic Applications: A Review", *Nanoscale Res Lett*, vol. 16, pp. 1741-27, 2021. https://doi.org/10.1186/s11671-021-03632-w
5. S. Tarantino, C. Capomolla, A. Carlà, L. Giotta, M. Cascione, C. Ingrosso, E. Scarpa, L. Rizzello, A.P. Caricato, R. Rinaldi, et al., "Shape-Driven Response of Gold Nanoparticles to X-Rays, *Nanomaterials*, vol. 13, pp. 2719-1-16, 2023. https://doi.org/10.3390/nano13192719
6. I. Tremi, S. Havaki, S. Georgitsopoulou, N. Lagopati, V. Georgakilas, V.G. Gorgoulis, A.G. Georgakilas, "A Guide for Using Transmission Electron Microscopy for Studying the Radiosensitizing Effects of Gold Nanoparticles In Vitro", *Nanomaterials*, vol. 11, pp. 859-1-19, 2021. https://doi.org/10.3390/nano11040859
7. P. Marinov, I. Petrov, K. Stoilov, T. Lazhovski, P. Temnishki, S. Simeonova, P. Georgiev, L. Mihaylov, E. Vassileva, K. Balashev, "UV-Visible Spectroscopy and Atomic Force Microscopy Analysis of Gold Nanoparticles Exposed to Varying Doses of Ionizing Radiation", *C. R. Acad. Bulg. Sci.*, vol. 78, no. 4, pp. 505-512, 2025. https://doi.org/10.7546/CRABS.2025.04.03
8. J. Turkevich, P.C. Stevenson, J. Hillier, "The Formation of Colloidal Gold", *J. Phys. Chem.*, vol. 57, no. 7, pp. 670–673, 1953. https://doi.org/10.1021/j150508a015
9. J. Kimling, M. Maier, B. Okenve, V. Kotaidis, H. Ballot, A. Plech, "Turkevich Method for Gold Nanoparticle Synthesis Revisited", *J. Phys. Chem. B*, vol. 110, no. 32, pp. 15700–15707, 2006. https://doi.org/10.1021/jp061667w
10. A. Bharti, K.H. Chae, N. Goyal, "Real-Time Synthesis and Detection of Plasmonic Metal (Au, Ag) Nanoparticles under Monochromatic X-Ray Nano-Tomography", *Sci Rep*, vol. 10, pp. 20877-1-11, 2020. https://doi.org/10.1038/s41598-020-77853-x
11. R.V. Lupusoru, D.A. Pricop, C.M. Uritu, A. Arvinte, A. Coroaba, I. Esanu, M.F. Zaltariov, M. Silion, C. Stefanescu, M. Pinteala, "Effect of TAT-DOX-PEG Irradiated Gold Nanoparticles Conjugates on Human Osteosarcoma Cells", *Sci Rep*, vol. 10, pp. 6591-1-14, 2020. https://doi.org/10.1038/s41598-020-63245-8
12. P. Georgiev, A. Bojinova, B. Kostova, D. Momekova, T. Bjornholm, K. Balashev, "Implementing Atomic Force Microscopy (AFM) for Studying Kinetics of Gold Nanoparticle's Growth", *Colloids and Surfaces A: Physicochemical and Engineering Aspects*, vol. 434, pp. 154–163, 2013. https://doi.org/10.1016/j.colsurfa.2013.05.064
13. S. Tarantino, A. Bianco, M. Cascione, A. Carlà, L. Fiamà, R.D. Corato, L. Giotta, P. Pellegrino, A.P. Caricato, R. Rinaldi, V. De Matteis, "Revolutionizing Radiotherapy: Gold Nanoparticles with Polyphenol Coating as Novel Enhancers in Breast Cancer Cells" – An In Vitro Study", vol. 20, no. 10, 2024. https://doi.org/10.1186/s11671-025-04186-x
14. Y.C. Dong, M. Hajfathalian, P.S.N. Maidment, J.C. Hsu, P.C. Naha, S. Si-Mohamed, M. Breuilly, J. Kim, P. Chhour, P. Douek, H.I. Litt, D.P. Cormode, "Effect of Gold Nanoparticle Size on Their Properties as Contrast Agents for Computed Tomography", *Sci Rep*, vol. 9, pp. 14912-1-13, 2019. https://doi.org/10.1038/s41598-019-50332-8